River, tide and morphology interaction in a macro-tidal estuary with active morphological evolutions

Xie, Dongfeng; Bing Wang, Zheng; Huang, Junbao; Zeng, Jian

DOI
10.1016/j.catena.2022.106131

Publication date
2022

Document Version
Final published version

Published in
Catena

Catena 212 (2022) 106131

Contents lists available at ScienceDirect

Catena

journal homepage: www.elsevier.com/locate/catena

River, tide and morphology interaction in a macro-tidal estuary with active morphological evolutions

Dongfeng Xie [a,*], Zheng Bing Wang [b,c], Junbao Huang [a], Jian Zeng [a]

[a] Zhejiang Institute of Hydraulics and Estuary, Hangzhou, China
[b] Faculty of Civil Engineering and Geosciences, Delft University of Technology, Delft, the Netherlands
[c] Deltares, Delft, the Netherlands

ARTICLE INFO

Keywords:
Tidal dynamics
River discharge
Tidal amplification
Morphological evolution
Qiantang Estuary

ABSTRACT

Understanding tidal dynamics in estuaries is essential for tidal predictions and assessments of sediment transport and associated morphological changes. Most studies on river-tide interaction ignored the influences of morphological evolutions under natural conditions such as the seasonal and interannual variations of river discharge. This study analyzes the multiple-timescale tidal dynamics in the Qiantang Estuary, a macro-tidal estuary in China with an extremely active morphological evolution. A large dataset including water levels at representative stations, river discharges and bathymetries since 1980 has been collected. The results of the analysis show that within a spring-neap cycle, the tidal amplification in the upper estuary is stronger during spring tide than during neap tide. This unexpected behavior is due to the high sediment concentration and the unique longitudinal profile of the estuary. On the seasonal and interannual timescales, the low water levels in the upper estuary depend on the local bathymetrical conditions. Tidal ranges in the upper estuary are larger in the high flow season and years, than in the low flow season and years, due to the erosion at high flow, in contrast to estuaries with less active morphological changes. During low flow season and years, the bed is gradually recovered, the low waters are elevated, and the tidal ranges decrease accordingly. A good relationship exists between the tidal ranges and the depth of the upper estuary. In the lower estuary, the flood dominance increases continuously due to embankment. In the upper estuary, the flood dominance is increased during the high flow periods, explaining the fast sediment input and bed recovery in the post high flow periods. A conceptual model of river-tide-morphology interaction of the estuary is proposed, which is also applicable for other shallow systems.

1. Introduction

Estuaries, transitional zones where a river meets the open sea, are worldwide surrounded by densely populated areas subject to fast economic development (Syvitski et al., 2009). Understanding tidal wave propagation and the corresponding spatial-temporal variations of the tide in estuaries is essential for tidal predictions and assessments of sediment transport and associated morphological changes. Water levels are probably the easiest data to measure in an estuary, and often the only oceanographic data available that extend back to time periods before the 20th century. They contain important information about the estuary and, therefore, implicitly provide a history of environmental change (Wang et al., 2019; Talke and Jay, 2019). From a coastal management point of view, they are of major practical significance for navigation, flood defense and provide information on salt intrusion and the estuarine ecosystem (Friedrichs and Aubrey, 1994; Kukulka and Jay, 2003a,b; Jay et al., 2011; Hoitink and Jay, 2016; Talke and Jay, 2019).

Although many studies have evaluated tidal distortion in different estuaries (e.g., Dronkers, 1986; Friedrichs and Aubrey, 1988; Wang et al., 2002; Bolle et al., 2010; Toublanc et al., 2015), river-tide interactions, mostly based on analytical or numerical models, have only recently gained attention, including Changjiang (Yangtze) River estuary and Pearl River estuary in China (Guo et al., 2015, 2019; Cai et al., 2015, 2020). Water level dynamics within estuaries are subject to various external forcing factors, such as basin geometry (length, convergence in width and bathymetry), river discharge influenced by hydrological variations in catchment areas, and oceanic tides. Depending on the balance between bed friction, estuarine convergence and river discharge, the incoming tides experience amplification, damping or remain constant in amplitude (Jay, 1991; Savenije, 2012). River

* Corresponding author at: Zhejiang Institute of Hydraulics and Estuary, Hangzhou 310020, China
E-mail address: dongfeng.xie@hotmail.com (D. Xie).

https://doi.org/10.1016/j.catena.2022.106131
Received 29 March 2021; Received in revised form 7 February 2022; Accepted 11 February 2022
Available online 17 February 2022

discharge is rarely constant and can vary rapidly over a large range, which induces a highly nonstationary behavior of tides in estuaries, especially into the landward direction (Guo et al., 2015; Jay et al., 2011; Kukulka and Jay, 2003a,b). A higher river discharge dissipates tidal energy, slows down tidal wave propagation and reduces the tidal range by enhanced bed friction (Godin, 1991; Cai et al., 2012; Zhang et al., 2015a). The river-tide interaction causes a higher mean water level during spring tide than during neap tide, explaining the fortnightly oscillations in mean water level (Matte et al., 2014). Most studies on river-tide interactions ignored the influences of morphological evolutions, because the bed level change over a short-term, e.g., spring-neap tidal cycle or seasonal timescale is limited with respect to the water depth.

Long-term changes in bottom friction, morphology and river discharge can modify tidal amplification and tidal asymmetry. Many studies have examined the long-term changes of tidal properties influenced by human activities, such as sand mining, land reclamation, channel deepening, bridges and weirs (Wang et al., 2002; Bolle et al., 2010; Zhang et al., 2010; Cai et al., 2012; Song et al., 2013; Winterwerp et al., 2013; Talke and Jay, 2019). However, few studies on river-tide interaction consider the influence of morphological evolution under natural conditions such as the seasonal and interannual variations of river discharge and tides, probably because in most estuaries the timescales of morphological evolution are much larger than those of the variations of hydrodynamic conditions.

There are some estuaries in the world with active seasonal or interannual morphological evolutions (Cooper, 2002; Shaw and Mohrig, 2014; Shimozono et al., 2019; Choi et al., 2020). It is necessary to explore the influence of the fast morphological evolutions on the tidal dynamics in such type of estuaries. The Qiantang Estuary, located at the East China Sea coast, is a typical example of the macro-tidal estuaries with active morphological evolutions (Fig. 1). The mean and maximum tidal ranges at Ganpu, the interface between the Qiantang Estuary and Hangzhou Bay, are 5.62 m and 9.0 m respectively (Han et al., 2003). The estuary is known for one of the strongest tidal bores worldwide. The swift tidal currents and river flood events result in substantial morphological changes on seasonal and interannual timescales. In several months, the local bed level changes can be more than 5 m (Chen et al., 1990; Han et al., 2003). In recent years, multiple studies have been carried out on tidal bore formation, propagation and turbulence properties (Pan et al., 2007; Pan and Huang, 2010; Tu and Fan, 2017), associated sediment transport and sedimentary sequence (Fan et al., 2014; Lin et al., 2005; Zhang et al., 2015b), based on field work and numerical modeling. The most remarkable morphological feature of the estuary is a large bar, a morphological bulge, elongating from the middle Hangzhou Bay landwards by 130 km (Fig. 1b). Several morphodynamic models have reproduced the formation of the large bar and its morphodynamic response to the large-scale embankment project since the 1960s (Yu et al., 2012; Xie et al., 2017a; Hu et al., 2018; Huang and Xie, 2020; Xie et al., 2021). Xie et al. (2018) found that the morphodynamic equilibrium of the estuary is maintained by the combination of two extreme hydrological conditions: tidal bore and river flood events. So far, no study focused on the tidal dynamics in the estuary, particularly on the interaction with fast morphological evolutions, has been carried out.

Based on the long-term bathymetrical data, together with data of water levels and river discharges, the present study investigates the tidal dynamics in the Qiantang Estuary. Specific objectives are: (1) to delineate the morphological evolutions under seasonal and interannual river discharge variations; (2) to analyze spatial-temporal variations of water levels and tidal amplifications on spring-neap, seasonal, annual and decadal timescales; (3) to link the tidal dynamics and morphological evolutions. The findings of this study are also relevant for other tidal systems with fast morphological changes.

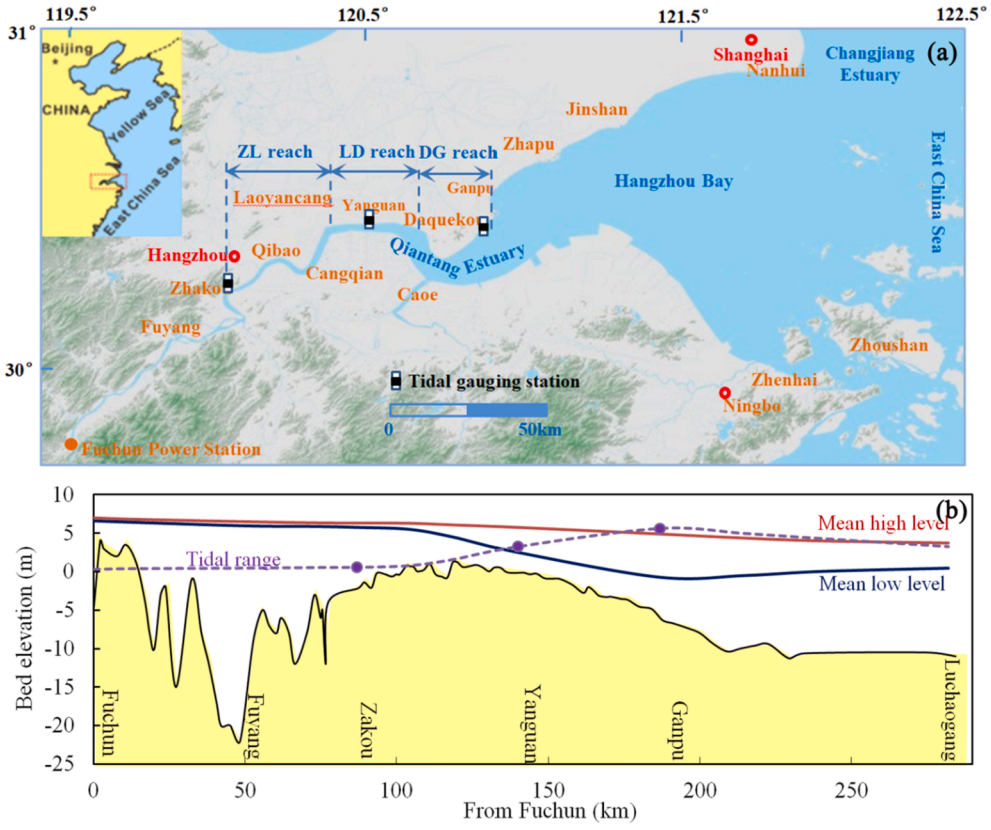

Fig. 1. (a) Location of Qiantang Estuary; (b) the lateral-averaged longitudinal bathymetries and the mean high and low tidal levels and tidal range along the estuary (after Xie et al., 2017a). The dots in panel b denote the locations of tidal stations of Zhakou, Yanguan and Ganpu.

2. Study area

With a total length of 386 km and a catchment area of about 60000 km^2, the Qiantang River is the largest river in the Zhejiang Province, China. The river debouches into the 120 km-long Hangzhou Bay, which has a funnel shape with the widths decreasing from 98.5 km at the bay mouth to 18.5 km at the bay head (Fig. 1a).

The Qiantang Estuary is usually divided into two reaches according to the hydrodynamic and morphological characteristics (Han et al., 2003). The riverine reach between Fuchun power station and the town of Zhakou is river-dominated with limited tidal influence. With the sediments mostly composed of gravel (2 - 30 mm) and coarse sand (0.05 - 0.5 mm), the morphology in the riverine reach is relatively stable (Han et al., 2003; Chen et al., 2006). The estuarine reach between the towns of Zhakou and Ganpu is controlled by the combination of river flow and tide, sedimented with silt and clay with a median grain size of predominantly 0.02 - 0.04 mm (Chen et al., 1990). This reach is dominated by the main part of the large longitudinal bar (Fig. 1b). The highest part of the bar is located between the towns of Cangqian and Qibao. It is more than 10 m higher than the estuary bottom at both the upstream and downstream sides of the bar. The Hangzhou Bay downstream of Ganpu, with an average depth of around 10 m, is dominated by tidal currents and the sediments are predominantly consisting of silt and clay (0.004 - 0.063 mm) (Editorial Committee for Chinese Harbors and Embayment (ECCHE), 1992). Tides from the East China Sea are dominated by the principal lunar semi-diurnal M_2 constituent. At the Hangzhou Bay mouth the mean tidal range is 3.2 m, gradually increasing landward to 5.62 m at Ganpu due to the strong convergence of width in the bay.

The current study, we focus on the estuarine reach of the Qiantang Estuary. According to the hydrographic and morphological characteristics, it can be divided into three sub-reaches. From Ganpu to Daquekou (DG reach) the width decreases from 18.5 to 5 km. Mean tidal range gradually decreases from 5.62 m to 3.28 m due to bed friction. It is located at the seaward slope of the large bar and the bed level rises from around -5 m at Ganpu to around -1 m at Daquekou. As a result, the tidal wave is seriously distorted. From Daquekou to Laoyancang (LD reach) the width decreases from 5 km to 2 km. The distorted tidal wave at this sub-reach eventually evolves into the world-famous tidal bore, where the bore height can be 1 - 2 m during spring tides (Han et al., 2003; Pan et al., 2007). From Zhakou to Laoyancang (ZL reach) the width is 1 - 2 km. The bed elevation shows a landward decreasing trend from 1 - 2 m to around -2 m. The tidal bore is gradually weakened and disappears. Mean tidal range at Zhakou is 0.58 m.

The mean discharge of the Qiantang River is 952 m^3/s (Han et al., 2003). The monthly averaged discharges vary between 319 and 1705 m^3/s (Fig. 2a). The runoff mainly occurs in the rainy season (between April and July), accounting for 55 - 60% of the annual runoff. During a river flood event, the discharge rises and falls sharply in several or more than 10 days, and the peak discharge can be more than 10000 m^3/s (Han et al., 2003). The flood events substantially correlate with the Asian summer monsoon as well as the local climate and other regional factors such as geographical variation and local sources of aerosols (Tian et al., 2012; Xia et al., 2016). Furthermore, it is characterized by the alternate wet and dry years on the interannual timescales, with the period around 20 years (Zeng et al., 2010). The sediment load from the Qiantang River correlates with the river discharge, varying between 1.4×10^6 - 14.2×10^6 ton/a, with the mean being 5.7×10^6 ton/a (Fig. 2b). The sediment in the Qiantang Estuary is mainly from the Changjiang Estuary. The huge sediment load from the Changjiang River, used to be around 4.5×10^8 ton/a, is diffused southward and enters the Qiantang Estuary - Hangzhou Bay system under the influence of the secondary Changjiang plume, especially in winter when the northwesterly winds prevail and the waves are relatively strong (Editorial Committee for Chinese Harbors and Embayment (ECCHE), 1992; Fan et al., 2017; Dai, 2021).

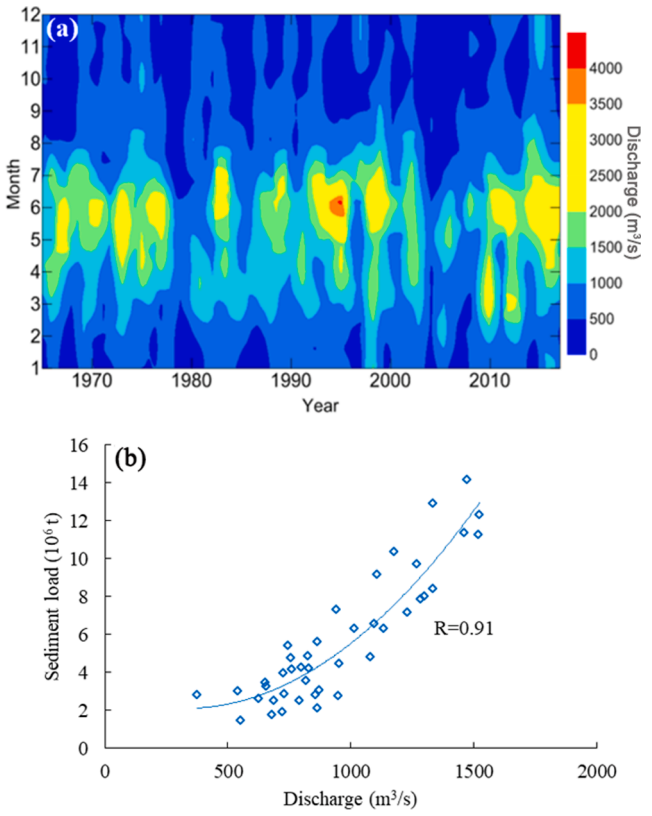

Fig. 2. (a) Monthly averaged discharges (m^3/s) and (b) annual sediment load - discharge rating curve of the Qiantang River. The data were collected from Zhejiang Hydrography Bureau, China.

3. Data and method

This study is based on three sets of data: bathymetry, water level and river discharge.

Bathymetry: Since the 1980s, the bathymetry in the estuarine reach has been measured uninterruptedly during the spring tide of every April, July and November by the Zhejiang Surveying Institute of Estuaries and Coasts (ZSIEC), representing bathymetries before (April) and after (July) the high flow season and after autumn (November), the season when the monthly maximum tidal ranges occur, respectively. The bed elevation along 60 cross-sections was observed using an Odom Hydrotrac echo-sounder. The error of the measured bed level is 0.1 m. After each survey, the channel volumes below multi-year averaged high water levels between cross-sections were calculated. The channel volumes of various sub-reaches and the cross-sectional averaged elevations are collected from ZSIEC. The bed elevation before 2000 was with respect to the theoretically lowest astronomical tidal datum at Wusong, whereas the subsequent surveys were with respect to the Chinese National Vertical Datum of 1985. In this study the elevations are unified in accordance with the 1985 datum.

Water level: High and low water levels of each tide (twice a day) at the Zhakou, Yanguan and Gaupu tidal gauging stations in the same period are collected from Zhejiang Hydrography Bureau (ZHB). The Zhakou and Ganpu stations are the landward and seaward boundaries of the estuarine reach of the Qiantang Estuary. Furthermore, the Ganpu station is the place where the maximum tidal range along the Qiantang Estuary – Hangzhou Bay system occurs (Fig. 1b). The reach downstream from Ganpu is dominated by width convergence and the reach upstream from Ganpu is dominated by bed friction. The Yanguan station is in the middle of the estuarine reach. The distances from Yanguan to Zhakou and Ganpu are both about 50 km.

River discharge: Daily river discharge from Fuchun power station in

the same period is collected from ZHB as well.

Water levels in shallow channels are related to local geometry, such as width and depth. Morphological evolutions in the Qiantang Estuary are extremely active and significantly influence the water levels. To link the morphological evolution and river discharge variations, relationships between the channel volumes of the two landward sub-reaches, e.g., the ZL and LD reaches and the average river discharge of the four months before the bathymetrical surveys are analyzed.

For the tidal dynamics analysis, the tidal range is determined as the difference between the high and low water levels. The mid-water level is the average of the high and low water levels. The tidal amplification factor is calculated as the ratio of the tidal ranges at Zhakou, at Yanguan to those at Ganpu. This approach of analysis is similar but not identical to the method of Munk and Cartwright (1966). Any changes in the tidal amplification factor provide information on changes of the physical conditions within the estuary (Wang et al., 2014, 2019; Jalón-Rojas et al., 2018). Especially, it can provide information of day-to-day changes.

For the seasonal and interannual tidal behavior analysis, we use the monthly averaged high and low water levels, tidal ranges and amplification factors. To clarify the controlling factors of water levels, the relationships between the tidal parameters at the upper stations and various external forces are established, such as the channel volumes of the sub-reaches and the tides at the seaward station Ganpu.

As tidal waves move into coastal and estuarine waters, a different high water propagation speed than low water leads to tidal wave deformation (Dronkers, 1986; Friedrichs and Aubrey, 1988). A shallow basin tends to cause flood dominance and a deeper basin tends to cause ebb dominance (Friedrichs and Aubrey, 1994). The tidal asymmetry is one of the factors generating residual sediment transport and is associated with morphological development. Tidal asymmetry is quantified using the method of Friedrichs and Madsen (1992):

$$F = \frac{5}{3}\frac{A}{H} - \frac{b-B}{B} \quad (1)$$

in which, A is the tidal amplitude, H refers to cross-section averaged channel depth, b is the total width (including tidal flats), and B is the width of the channel. If $F>0$, the time variations in channel depth are more important than time variations in channel width, leading to a flood-dominant tide and a tendency for landward sediment transport; if $F<0$, the opposite holds, resulting in an ebb-dominant tide.

4. Results

4.1. Morphological evolutions

The morphological evolution of the estuary and its relationship with river discharge are analyzed first, providing a basis for the tidal dynamics analysis. Fig. 3 illustrates time series of the average river discharge of the four months before each bathymetrical survey and the channel volumes of the three sub-reaches in the months of April, July and November from 1980 to 2018. The annual averaged discharge varies between 370 m^3/s and 1390 m^3/s. Two periods of continuous dry years (1980 - 1988 and 2003 - 2009), and two periods of continuous wet years (1989 - 2002 and 2010 - 2018) can be roughly distinguished. In the dry years the Qiantang River basin experienced relatively light precipitation whereas in the wet years it received sufficient precipitation (Xia et al., 2016). The mean discharges of the four periods are 801, 1022, 630 and 1123 m^3/s, respectively. The average discharges of the periods before the three bathymetrical surveys during 1980 - 2018 are 831, 1448 and 623 m^3/s, respectively. The discharges in the high flow seasons are larger than the bed formation discharge of the Qiantang estuary, 1100 m^3/s (Chen et al., 2006; Xie et al., 2017a), and can amount to about twice of those in the low flow seasons.

The channel volumes of the ZL reach in April, July and November vary between 1.38×10^8 and 3.16×10^8 m^3, 1.54×10^8 and 3.99×10^8 m^3, 1.45×10^8 and 3.00×10^8 m^3, respectively, with the average being 2.22×10^8 m^3, 2.79×10^8 m^3 and 2.28×10^8 m^3, respectively (Fig. 3b). The channel volumes of the LD reach in April, July and November vary between 0.93×10^8 and 2.60×10^8 m^3, 1.14×10^8 and 2.93×10^8 m^3, 1.11×10^8 and 2.47×10^8 m^3, respectively, with the average being 1.86×10^8 m^3, 2.19×10^8 m^3 and 1.72×10^8 m^3, respectively. Averagely, the channel volumes of the two sub-reaches in July are 20 - 25% larger than in April and November. The channel volumes of both reaches correlate with the average discharge prior to the bathymetrical surveys (Fig. 3c). This is consistent with the findings of Xie et al. (2018) who found that channel volume upstream of Yanguan in July correlates well with the river discharge between April and July. The cross-sectional area and the cross-section averaged depth of estuaries are power functions of the river discharge (Smith, 1974; Han et al., 2009). Since the mean river discharges during last November to April and during July to November are comparable (Fig. 3a), overall, the channel volumes in both reaches are also comparable in April and November. The high discharge from April to July results in the largest channel volume in July. Furthermore, the channel volume - discharge correlation for the ZL reach is better than for the LD reach, indicating that the role of river discharge is more important in the upper reach. It should be noted that the channel volume in July is mainly related to bed erosion caused by high discharge, especially by river flood events, whereas in April and November the channel volume is related to accumulation after a high flow season, due

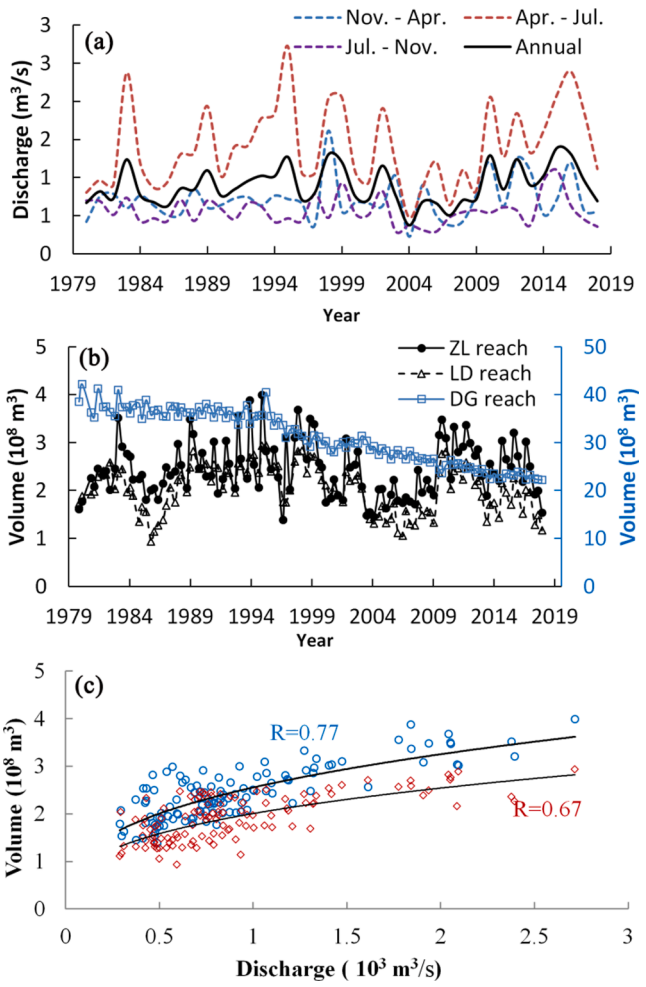

Fig. 3. (a) The average river discharge in the four months before the bathymetrical surveys in April, July and November, (b) the channel volumes below local annual highwater levels of the three sub-reaches of the estuary, (c) relationships of the channel volumes of the ZL and LD reaches and the average river discharge in the four months before bathymetric measurements.

to sediment input by tidal currents (Han et al., 2003; Xie et al., 2018). Moreover, the volume in April and November also depends on the channel volume of last measurement. For example, the channel volume of the ZL reach in November 2010 is 2.89 × 10^8 m^3, much larger than the predicted value by the fitted curve in Fig. 3c, despite the average discharge between August and November of 2010 is only 538 m^3/s. This is because the channel volume in July 2010 is large, being 3.48 × 10^8 m^3.

The average volumes of the ZL and LD reaches are 25% larger in the wet years than in the dry years. For example, the averages volume of the ZL reach in the periods of 1980 - 1988, 1989 - 2002, 2003 - 2009 and 2010 - 2018 are 2.33 × 10^8, 2.64 × 10^8, 1.96 × 10^8 and 2.65 × 10^8 m^3. Furthermore, extreme values of channel volumes can be observed. 1995 and 2004 are the rainiest and driest years in the last decades, respectively (Lin et al., 2012; Xia et al., 2016). As a result, extreme high and low annual river discharges occurred in the two years being 1390 and 370 m^3/s, respectively. Correspondingly, the sum volumes of the two reaches in the two years are largest and smallest, being 6.05 × 10^8 and 2.91 × 10^8 m^3, respectively.

The seasonal and interannual variations in the channel volume of the DG reach are opposite to the other two reaches. The average volumes of this reach in April, July and November since 1980 are 31.14 × 10^8, 30.37 × 10^8 and 31.55 × 10^8 m^3, respectively. This is related to the sediment exchange between the three sub-reaches. During the high discharge periods, the sediment eroded from the ZL and LD reaches is transported seaward and accumulated at the DG reach, and vice versa during the low discharge periods (Chen et al., 1990; Han et al., 2003; Xie et al., 2018). The most remarkable change in the DG reach is that the volume has been decreased continuously from 38.89 × 10^8 in 1980 to 22.24 × 10^8 m^3 in 2018. This is related to the large-scale embankment project gradually implemented in the Qiantang Estuary and Hangzhou Bay which has reduced the tidal prism of the estuary and enhanced the sediment input (Han et al., 2003; Xie et al., 2021).

Fig. 4 shows the magnitudes of the cross-section averaged bed level changes of the neighboring bathymetrical surveys since 1980. The changes in the ZL and LD reaches are relatively large, varying between -3 and 3.5 m; those in the DG reach vary between -2 and 2.5 m. As previously reported (e.g., Chen et al., 1990; Xie et al., 2018), the local bed level changes can be even larger than these cross-section averaged values.

4.2. Temporal and spatial changes of tidal dynamics

Fig. 5 illustrates an example of fortnightly water levels at Zhakou, Yanguan and Ganpu stations in October 2018. The monthly river discharge is 759 m^3/s, and no river flood events, nor storm surge occurred. At the seaward station Ganpu, the high and low water levels vary between 3.69 m and 6.90 m and between 0.47 m and -1.33 m, respectively. Accordingly, the tidal range varies between 3.31 m and 8.06 m. At Yanguan, the highwater level varies between 4.09 m and 7.73 m, whereas the variation of the low water level is insignificant, fluctuating around 2.33 m with an amplitude of change less than 0.3 m. Accordingly, the tidal range varies between 3.31 m and 4.90 m (Fig. 5c). According to Talke and Jay (2019), within a tidal river, the lowest water levels occur during neap rather than spring tides, because a larger tide increases the friction felt by river flow, and the point where the lowest low waters begin to be during neap tides is the seaward boundary of the tidal river. Thus, the reach upstream from Yanguan can be defined as a tidal river. The tidal range at Yanguan correlates positively with the tidal range at Ganpu, whereas the amplification factor fluctuates around 0.6 and is not influenced by the tidal range at Ganpu except that it increases with the tidal range at Ganpu during the neap tides (Fig. 5b, d). The high and low water levels at the landward station Zhakou vary between 4.12 m and 8.36 m, and between 4.19 m and 5.84 m, respectively. Both highest high and lowest low levels appear in the spring tides. The tidal range varies between 0.04 m and 2.52 m and the amplification factor varies between 0.01 and 0.32, both correlating positively with the tidal range at Ganpu (Fig. 5c, d).

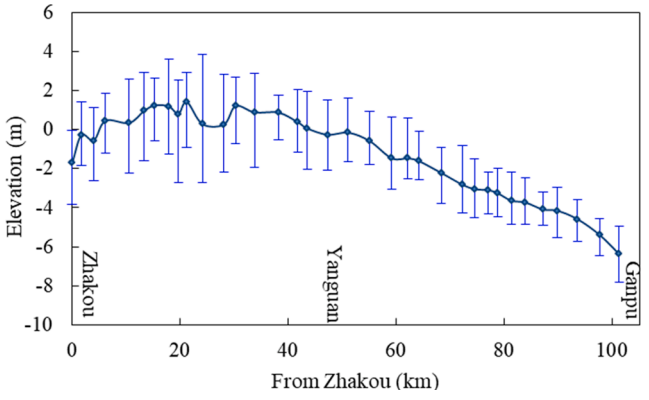

Fig. 4. The amplitudes of the cross-sectional bed level changes of the neighboring bathymetrical surveys since 1980. The solid line denotes the longitudinal profile of the estuary, and the error bars reflect the maximal bed erosion and accumulation.

As morphology and river discharge also influence the tidal wave propagation, a longer - term comparison is made for different channel volume classes. The tidal ranges at the three stations in April, July and November since 1980 are chosen, matching the periods of the bathymetric data. River flood events can significantly influence water levels and morphology. To avoid this complication, for each channel volume class the tidal data during river flood events are filtered out. Furthermore, the channel volume of the Zhakou - Yanguan reach is used since the channel volumes of the sub-reaches in the upper estuary show similar variations (Fig. 3). For the same channel volume class, the tidal ranges and the amplification factors correlate positively with the tidal range at Ganpu, except that the amplification at Yanguan fluctuates around a certain value if the tidal range at Ganpu is relatively large (Figs. 6 and 7), consistent with the results of the fortnightly variations in Fig. 5. On the other hand, the larger the channel volume is, the larger the tidal ranges and amplifications in the upper estuary are. For example, under the tidal range at Ganpu of 8.0 m, the tidal range at Zhakou is 2.55 m, 2.02 m, 1.71 m, 0.96 m, and the amplification is 0.32, 0.25, 0.21 and 0.12 for the various channel volume classes in decreasing order.

Fig. 8 illustrates monthly average high, low and mid-water levels, tidal ranges at Zhakou, Yanguan and Ganpu and tidal amplifications at the former two stations. At Ganpu the variations of the monthly low level are limited, fluctuating around -0.60 m. The highwater level shows significant seasonal variations. Moreover, it shows an increasing trend, especially since 2007. The low level at Yanguan varies between 0.88 and 5.34 m, much more significantly than the low level at Ganpu. Most of the lowest low levels occur in July, corresponding to the maximum monthly river discharge which results in significant bed erosion. Furthermore, the low level is higher in the dry years than in the wet years. In the four periods of continuous dry and wet years, the mean low levels at Yanguan are 3.30, 2.26, 3.27 and 3.02 m, respectively. The low water levels at Yanguan correlates with the channel volume of the LD reach (Fig. 9), indicating that the low levels in the upper estuary depend on local bathymetries. The highwater level at Yanguan correlates with that of Ganpu whereas its relationship with the river discharge is insignificant (Fig. 9c, d). The low level at Zhakou varies between 4.33 and 6.97 m, showing the similar seasonal and interannual variations with that at Yanguan. The correlation between the low levels at Zhakou and the channel volume of the ZL reach is even better than at Yanguan (Fig. 9a). The highwater level at Zhakou depends on the variation of the river discharge whereas its relationship with the high level at Ganpu is insignificant.

The mid-water levels and tidal ranges at the Yanguan and Zhakou also show significant seasonal and interannual variations (Fig. 8c, d).

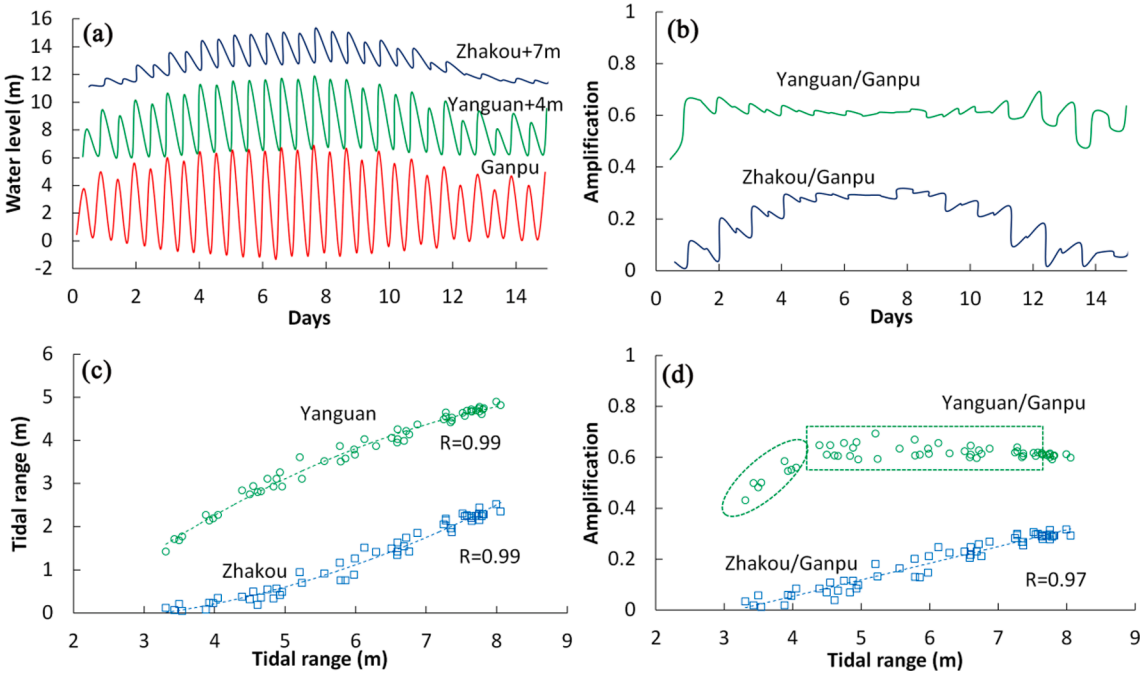

Fig. 5. Time series of water levels at Zhakou, Yanguan and Ganpu in October 2018 (a), and the corresponding amplification factors (b). The relationships between the tidal ranges (c) and the amplifications (d) at Zhakou and Yanguan and the tidal range at Ganpu.

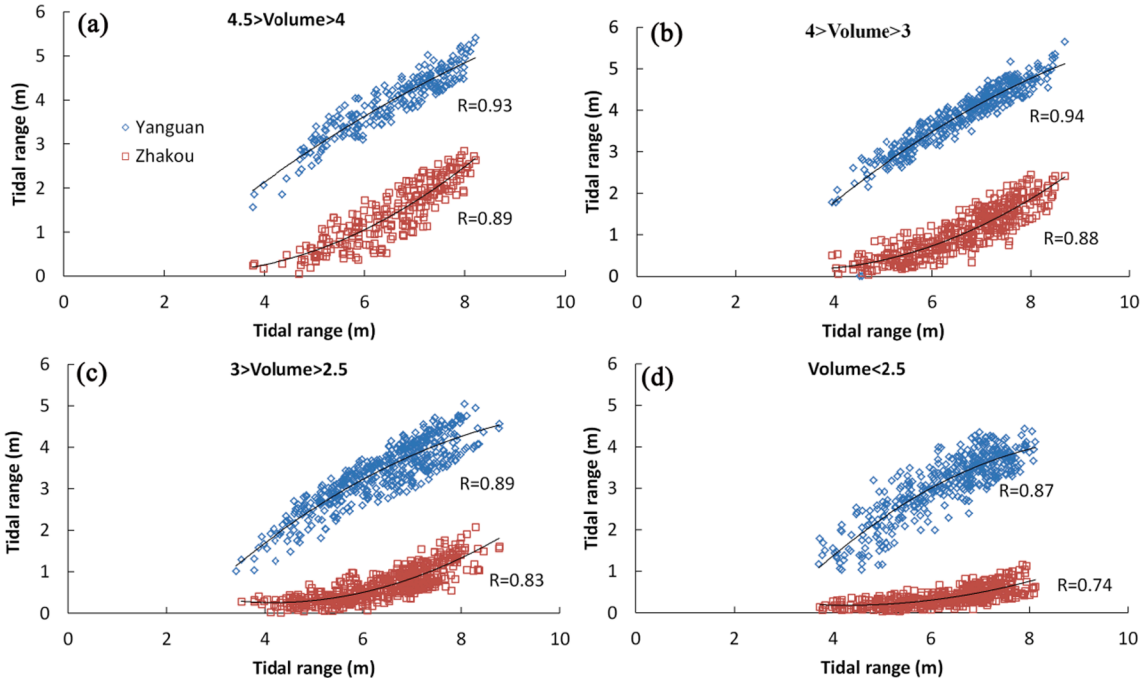

Fig. 6. Relationships between the tidal ranges of Zhakou and Yanguan and the tidal range at Ganpu in various channel volume classes of the Zhakou - Yanguan reach. The unit of channel volumes is 10^8 m^3, the same below.

The mean tidal range at Yanguan is 2.53 and 3.42 m in the periods of continuous dry and wet years, respectively. Accordingly, the mean amplification factor is 0.45 and 0.58 in the periods of continuous dry and wet years, respectively. Similarly, the mean tidal range at Zhakou is 0.44 and 0.82 m in the periods of continuous dry and wet years, respectively. Accordingly, the mean amplification factor is 0.18 and 0.24 in the periods of continuous dry and wet years, respectively. Overall, the amplification factors at the two stations in the wet years are about 30% larger than in the dry years. Both tidal ranges and amplifications at Zhakou and Yanguan correlate positively with the local channel volumes (Fig. 10).

The metric of tidal asymmetry *F* at the three stations are positive, indicating that the tide in the estuary is flood dominant. At Ganpu *F* has increased from 0.47 to 0.87, with the most apparent increase occurring after 2007 (Fig. 11a), simultaneously with the increase of the highwater level. There exists good relationship between *F* and the local channel volume (Fig. 11b). *F* at Yanguan varies between 0.62 and 1.61, with the average being 0.99, much larger than many other estuaries. For

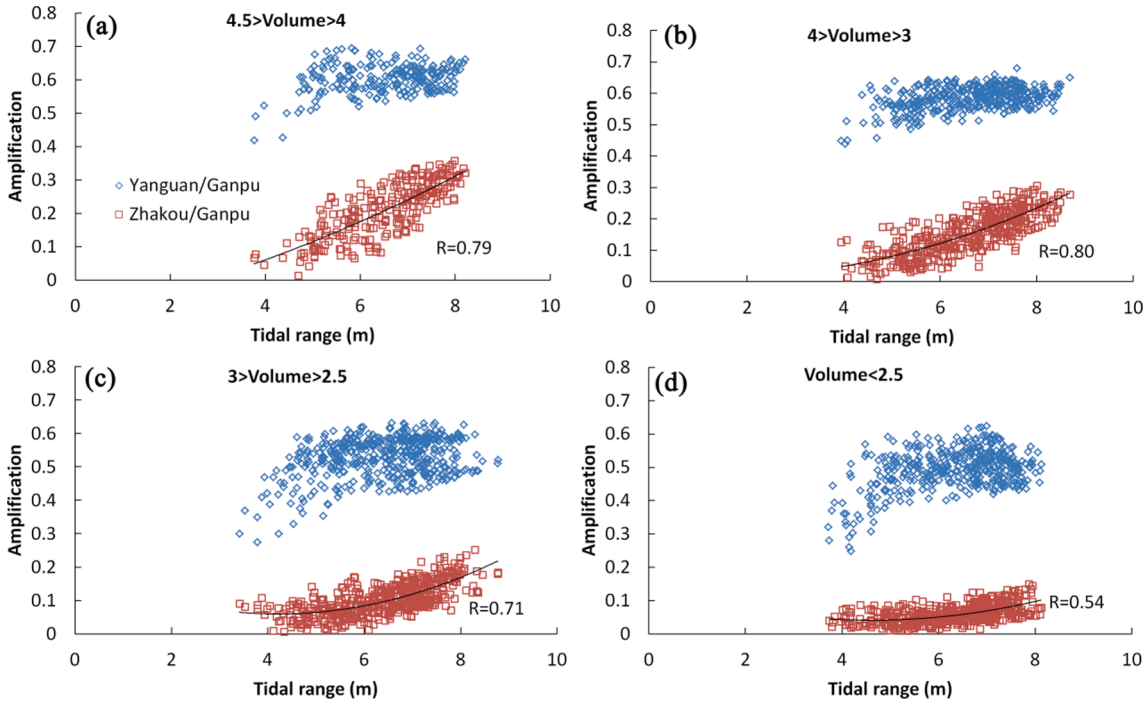

Fig. 7. Relationships between the amplification factor at Zhakou and Yanguan and the tidal range at Ganpu in various channel volume classes of the Zhakou - Yanguan reach.

example, in the upper Pearl estuary in southern China, *F* is around 0.30 (Cao et al., 2020). The large *F* at Yanguan is related to the occurrence of the biggest tidal bore worldwide, which is an extreme case of tidal wave deformation. At Zhakou *F* varies between 0.06 and 0.25, with the average being 0.14. The tidal asymmetries at Yanguan and Zhakou show opposite relationship with the variations of river discharge. In the low flow periods, *F* at Zhakou decreases while *F* at Yanguan increases, and vice versa in the high flow periods. In the high flow periods, the larger channel volume of the upper Qiantang Estuary results in an increase of tidal range at Zhakou and the landward penetration of the incoming tides. At Yanguan, the influence of the channel volume changes is relatively small.

5. Discussion

5.1. The river-tide-morphology interaction

River-tide properties can vary in systems subject to strong fluctuations of river discharge. The effects of river flow on tidal dynamics are known, mostly based on analytical solutions or numerical models (Godin, 1991; Kukulka and Jay, 2003a,b; Jay et al., 2011; Sassi and Hoitink, 2013; Cai et al., 2015, 2020). There are basically four direct influences of high river discharge: (1) increased ebb currents, favoring the growth of overtides and causing tidal damping; (2) increased water levels and water depths, which means lowering the bed resistance; (3) changed hydraulic drag via changing of suspended sediment concentrations; (4) bed level change. Until recently, the impacts of river discharge on tidal decay and deformation were investigated using time series of real observations (Wang et al., 2014, 2019; Jalón-Rojas et al., 2018). Concerning tidal range and amplification, a higher river discharge corresponds to a smaller tidal range and thus weaker amplification in the upper estuary. For example, the tidal range in the upper Yangtze can be 1.7 to 7.5 times higher during dry periods than during wet periods (Guo et al., 2015). Similar relations were found in the upper Scheldt Estuary and the Gironde Estuary (Wang et al., 2019; Jalón-Rojas et al., 2018). Because seasonal or interannual morphological evolutions in most estuaries are insignificant unless the natural systems are strongly disturbed by human activities, few have considered the role of natural morphological evolutions on the tides. In fact, the erosion / accumulation rate of the Qiantang Estuary is at least an order of magnitude greater than those documented from other tide-dominated estuaries, where the evolution cycle takes place over decades (Wang et al., 2002; Dalrymple and Choi, 2007; van der Wal et al., 2002; Wang et al., 2019; Luan et al., 2016; Jalón-Rojas et al., 2018; Cao et al., 2020). It is necessary to consider the role of morphological evolution on the tidal dynamics in the Qiantang Estuary.

In the Qiantang Estuary, the effects of river discharge in different reaches can be different. The highwater level at Zhakou can be elevated by the high river discharge, but the highwater level at Yanguan depends predominantly on the highwater level of the incoming tides (Fig. 8, 9). At the upper reach, the high discharge induces significant bed erosion and subsequently a larger channel volume. Correspondingly the low water levels at Zhakou and Yanguan are lowered. The eroded sediments are transported seaward and accumulated at the lower reach during a high discharge period. Thus, the low water levels at the two upstream stations correlate with the local channel volumes (Fig. 9a, b), but their relationship with the river discharge is insignificant. The high and low water levels at Ganpu are hardly influenced by river discharge because of the larger width and depth (Fig. 8). The damping effect of high river discharge on the tidal ranges at Zhakou and Yanguan is insignificant, probably because the bed erosion by a high river discharge is fast. Bed erosion occurs basically synchronously with river flood events. Meanwhile, the periods of river flood events of the Qiantang River usually last several days to half month (Han et al., 2003; Xie et al., 2018). The damping effect of high discharge on the tidal range was smoothed because we focused on the monthly averaged data. The effect of tidal amplification induced by the high discharge is larger at the upstream station than at the downstream station. The average tidal ranges at Zhakou and Yanguan in the periods of continuous wet years are 1.86 and 1.35 times those in the periods of continuous dry years, respectively (Fig. 8c).

The low discharge during dry season or years exerts different effects from the high discharge on the tidal dynamics. Under low discharge condition, sediment accumulation occurs in the upper estuary because

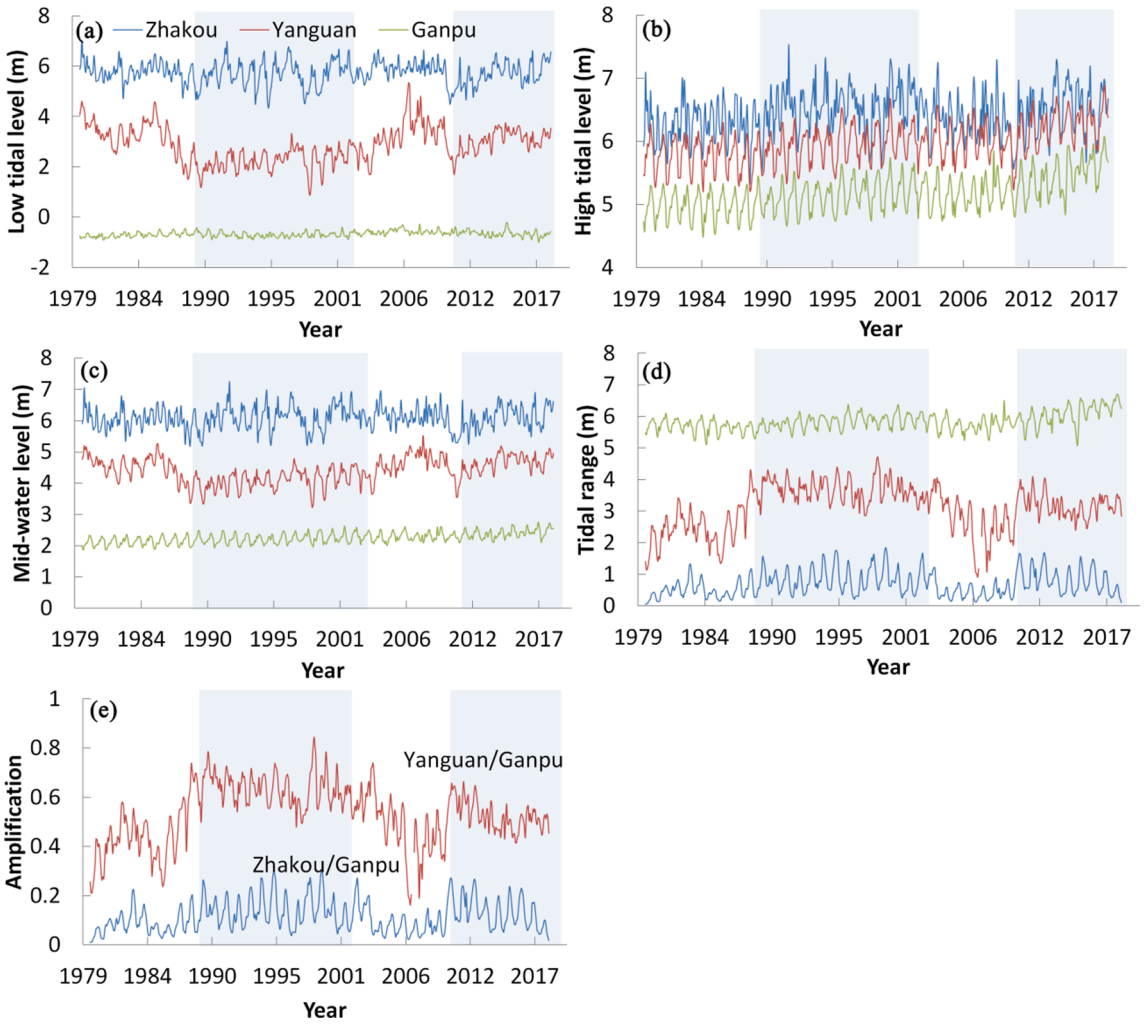

Fig. 8. The monthly low and highwater levels (a, b), mid-water levels (c), tidal ranges (d) at the three stations and the corresponding amplifications (e). The shades denote the continuous wet years.

of the sediment input by tides, especially by the tidal bore (Xie et al., 2018). Results in this study showed that the increased channel volumes upstream Daquekou by the high river flow amplify the tide and enhance the flood dominance (Fig. 11), favoring the sediment input after the high discharge period. A positive relationship exists between the sediment accumulation from July to November and the sum volume of the ZL and LD reaches in July (Fig. 12). Larger channel volumes in the two reaches mean a faster sediment accumulation in the post high-discharge periods. With sediment accumulation in the upper estuary, the low water levels increased accordingly, and the tidal amplification and flood dominance decreased gradually. Subsequently, sediment input decreases gradually. Thus, a dynamic morphodynamic equilibrium can be maintained. A conceptual model of the river-tide-morphology interaction of the estuary is summarized in Fig. 13.

The influences of human-induced morphological changes on tides have been evaluated in many estuaries. For example, mainly due to continuous channel deepening, the Ems Estuary experienced a tidal range increase of 125% at the mouth between 1950 (1.6 m) and 2010 (3.6 m), and a transition of suspended sediment concentration from low (~1 kg/m^3) to high (>10 kg/m^3) (van Maren et al., 2015; Winterwerp and Wang, 2013; Dijkstra et al., 2019). The tidal ranges of the upper region of the Pearl Estuary increased from 0.35 m in 1990 to 0.53 m in 2005 due to the uncontrolled sand mining, enhancing the tidal dynamics (Zhang et al., 2010), but reducing the flood-dominant tidal asymmetry (Cao et al., 2020; Zhang et al., 2018). The role of bed erosion by high river flow in the Qiantang Estuary is similar to the effect of dredging and sand mining. However, the natural erosion of the Qiantang Estuary can be gradually recovered in several months or years because of the ample sediment supply and the strong tidal currents after the flood events. Human activities also exert influences on the morphology of the Qiantang Estuary. Since the 1960s a large-scale embankment project has been implemented seaward progressively, aiming at improving flood protection and navigation (Han et al., 2003). Upstream Daquekou the embankment was basically finished before the 1970s and the morphdynamic system has reached a new dynamic equilibrium (Han et al., 2003; Xie et al., 2017b). The channel volumes in the ZL and LD reaches mainly depend on the variations of the river discharge. The embankment in the DG reach was finished in the 2010s. The embankment decreases the tidal prism, enhances sediment accumulation and hence the channel volume in this reach decrease continuously (Fig. 3b). The morphological response still continues at present. The influence of the morphological evolution on the low water level at Ganpu is insignificant. The highwater level has increased due to the enhanced reflection of tidal wave by seawall (Han et al., 2003; Xie et al., 2017b; Zeng et al., 2017; Pan et al., 2019). As a result, the tidal range at Ganpu has increased by about 0.5 m (Fig. 8).

5.2. *Reasons for the 'abnormal' tidal amplification variations*

Usually, a larger tidal range in an estuary induces larger bed friction.

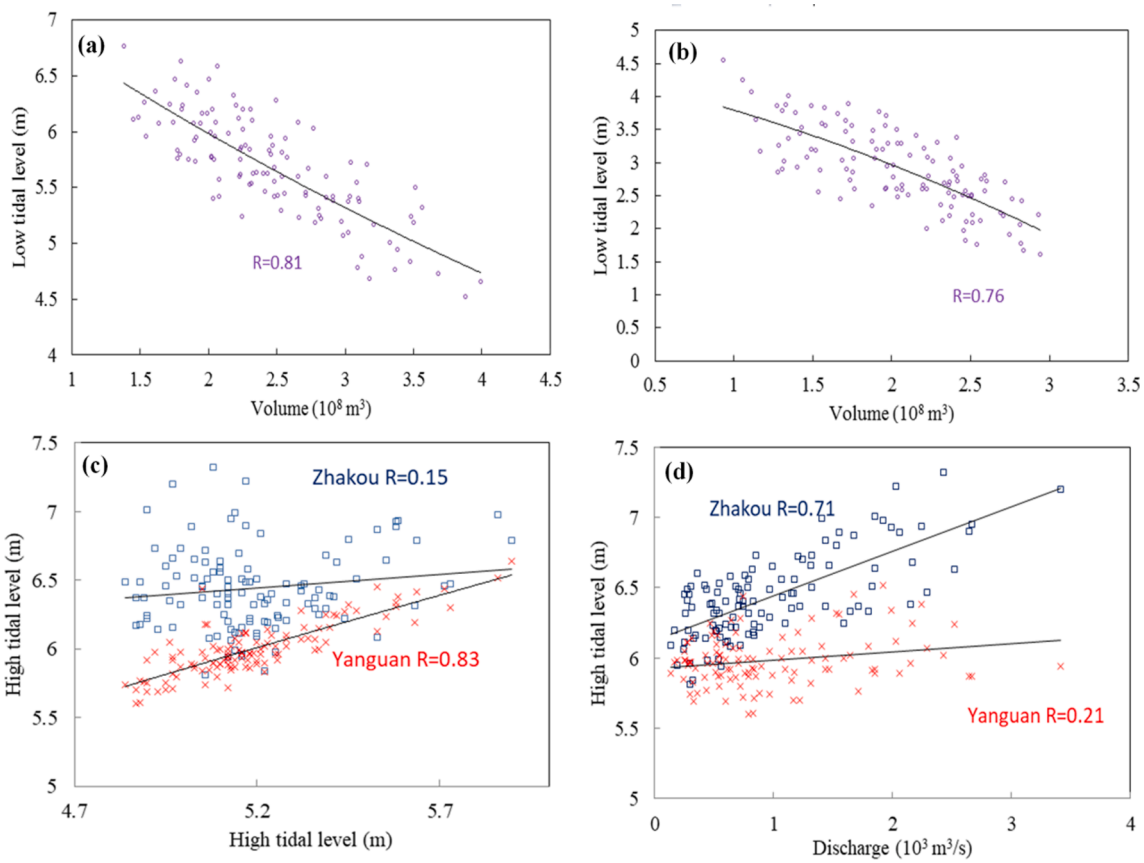

Fig. 9. Relationships between the monthly low water levels at Zhakou (a) and Yanguan (b) and channel volumes of the ZL and LD reaches, respectively, and the monthly highwater levels at Zhakou and Yanguan and highwater level at Ganpu (c) and the monthly river discharge (d), respectively.

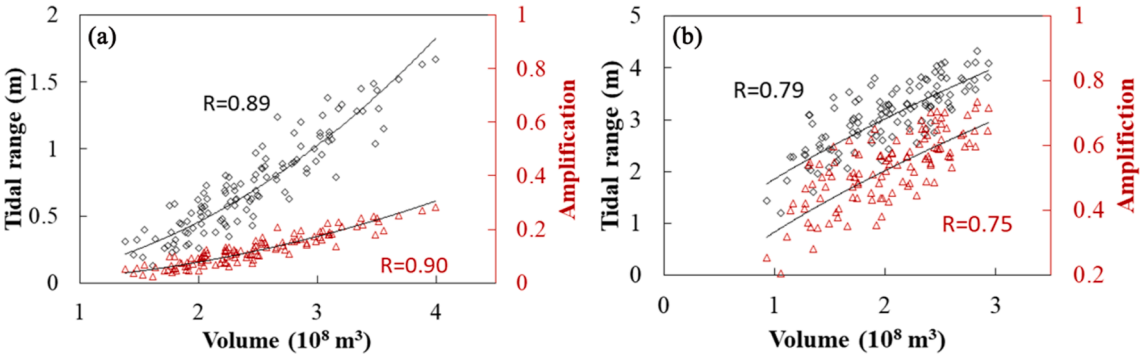

Fig. 10. Relationships between monthly tidal ranges and amplifications at Zhakou (a) and Yanguan (b) and the channel volume of the ZL and LD reaches, respectively.

Hence tidal amplification at the upstream station correlates negatively with the tidal range at the downstream station (Jalón-Rojas et al., 2018; Wang et al., 2019). In the Qiantang Estuary, tidal amplifications at both Zhakou and Yanguan correlate positively with the tidal range at Ganpu. This 'abnormal' tidal behavior is probably related to the unique hydrographic and morphological characteristics of the estuary. The Yanguan reach is the place where the biggest tidal bore in the world occurs, and current velocity can be as high as 6 m/s and strong turbulence occurs. As a result, the suspended sediment concentration (SSC) during spring and intermediate tides are large, with the maximal SSC more than 15 kg/m^3 (Pan and Huang, 2010; Tu and Fan, 2017). A high SSC can decrease the effective hydraulic drag (Winterwerp et al., 2013; Wang et al., 2014). Furthermore, the larger the SSC, the more kinetic energy is extracted from the water to be translated into potential energy, in order to maintain the high SSC (Burchard and Schuttelaars, 2012; Li et al., 2018). Therefore, during spring and intermediate tides, the increase of tidal amplification at Yanguan with the tidal range at Ganpu is insignificant (Fig. 3b and Fig. 4).

At Zhakou, the tidal bore is weak. Only undular bore can be observed during spring tides and no bore is formed during neap tides (Pan et al., 2007). Recent field work showed that the maximal SSC in the upper estuary is 0.81, 3.7 and 0.95 kg/m^3 in April, July and November of 2018, respectively (Fig. 14). In other words, the upper estuary is characterized by low turbidity, comparable with other shallow systems. Therefore, the positive correlation between the amplification at Zhakou and the tidal range at Ganpu cannot be explained by the SSC effects. Instead, the abnormal amplification is probably related to the development of the large longitudinal bar (Fig. 1b) and the variation of the water depth with

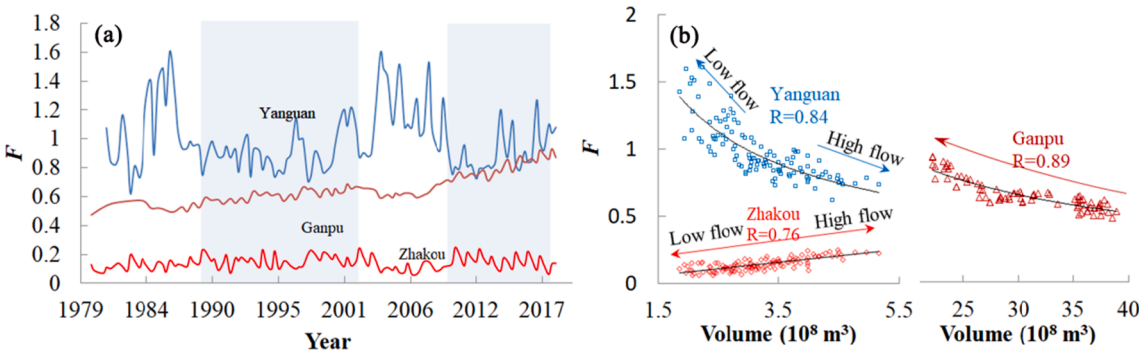

Fig. 11. Metric of tidal asymmetry *F* at the three stations in April, July and November since 1980 (a), and the relationships between *F* and the channel volumes (b).

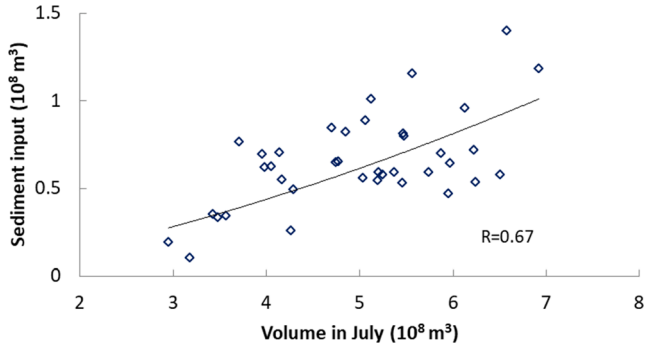

Fig. 12. The relationship between the sediment accumulation from July to November and the sum volume in July in the ZL and LD reaches.

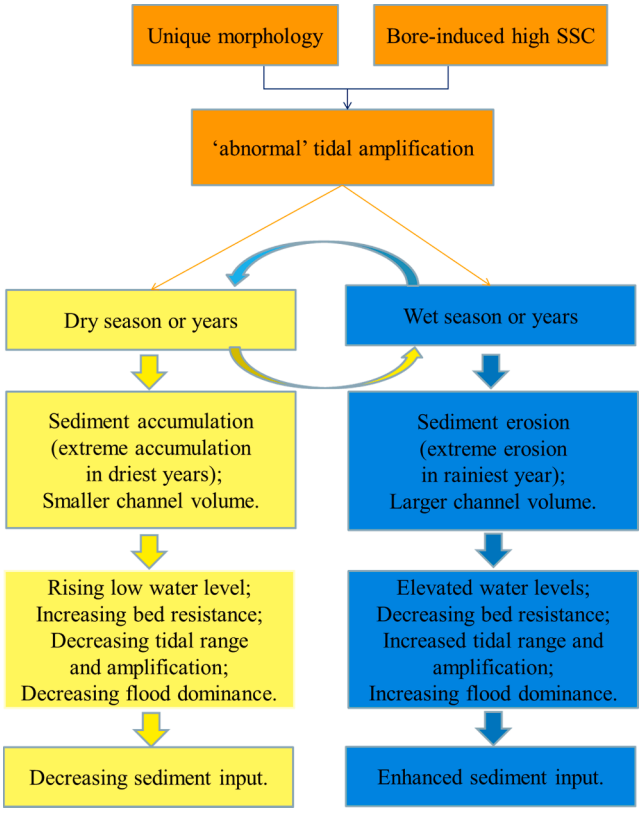

Fig. 13. A conceptual model of the river-tide-morphology interaction in the estuary.

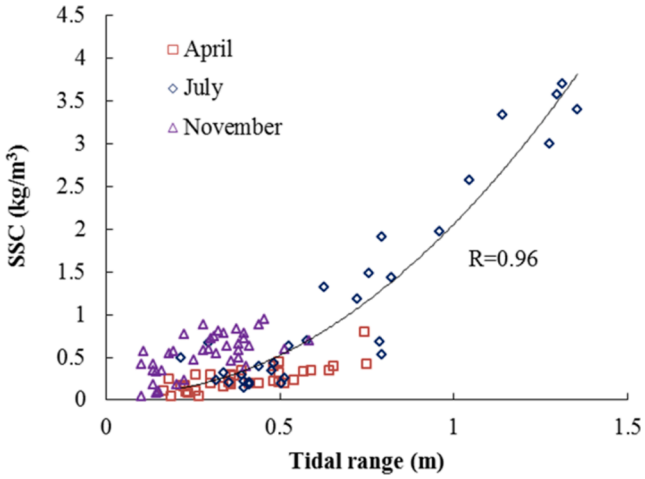

Fig. 14. The relationships between the maximal depth-averaged SSC at Qibao and tidal range at Zhakou in April, July and November of 2018 (modified from Xie et al., 2020).

the tidal range. The bed elevation lowers landwards from 1 - 2 m at the bar apex at Qibao to around -2 m at Zhakou. Under the annually average low water levels, the water depth appears smallest at Yanguan, being 2.60 and increases landwards, being 7.89 m at Zhakou. The landward increasing water depth in the Qiantang Estuary contrasts with the generally landward decreasing trend in water depth (Cai et al., 2012; Hoitink and Jay, 2016; Wang et al., 2014; Hoitink et al., 2017; Wang et al., 2019; Talke and Jay, 2019), and due to the development of the large longitudinal bar (Fig. 1b), friction effects decrease with the water depth. Meanwhile, the landward increase of water depth also reduces the hydraulic drag (Godin, 1991; Jay et al., 2011; Wang et al., 2019).

Talke and Jay (2019) identified two types of systems that are particularly prone to tidal amplification: (a) shallow, strongly damped systems, in which a small increase in depth produces a large decrease in effective friction, and (b) systems in which wave reflection and resonance are strongly influenced by changes to depth, friction, and convergence. Apparently, the Qiantang Estuary belongs to the former. During a short-term cycle with a normal hydrograph, e.g., the spring-neap cycle, the morphological evolution is limited, but the water depth increases with increasing tidal range because stronger tidal flow causes more resistance to the river flow. The amplifications at Yanguan and Zhakou are determined by two different physical mechanisms. At Yanguan the high SSC effect is more important, whereas at Zhakou the effect of the variation of water depth in the upper estuary is dominant.

On the longer timescale, the morphological evolutions play an important role on the amplification, especially due to the shallow depth. With the morphological evolutions in the upper reach, the magnitudes of the monthly mean amplification factors at Zhakou and Yanguan are 0.01

- 0.30 and 0.16 - 0.84, respectively. The bed level changes induced by the variation of river flow induce the changes of water levels and amplification of the tidal ranges (Fig. 8-10). Furthermore, the monthly water depths under mid-water levels in the upper estuary correlate well with local bed elevations (Fig. 15). The increasing water depths with the bed erosion by high flow reduce the hydraulic drag and favor the amplifications.

5.3. Implications

In this study, we have evaluated the evolutions of vertical tides in the Qiantang Estuary. In fact, the sediment transport and morphological evolution are mainly governed by horizontal tides. However, the asymmetry of the vertical tide can be a good indicator of the asymmetry of the horizontal tide (Wang et al., 2002; Zhou et al., 2018). As shown in Fig. 13, the SSC in the upper estuary correlates well with the tidal range. Over the post high-flow periods, the larger tidal range and tidal storage have contributed to an intensification of tidal pumping and an increase of the SSC. Given that SSC decrease gradually upstream from Yanguan (Han et al., 2003), it can be understood that the estuarine turbidity maximum shifts landwards. In turn, during the low flow seasons or years, the tidal range and horizontal velocities decrease, and the turbidity maximum shifts seawards. The cyclic seasonal and interannual transition of the hydro-sedimentary conditions has profound consequences for the estuary, as high SSC is associated with a strong reduction in oxygen levels (Uncles et al., 1998; Talke et al., 2009) and primary production (Cloern, 1987; Kukulka and Jay, 2003a,b; Gao and Wang, 2008).

The present study has its methodological implications. Studies in recent years based on analytical and numerical models (e.g., Kukulka and Jay, 2003a,b; Cai et al., 2012, 2015) or on nonstationary harmonic methods (Guo et al., 2015, 2019; Cao et al., 2020) have largely improved our understanding on the river-tide interaction. However, none of these studies takes the joint effects of variations of river flow and morphology into account. Findings from this study reveal that the tidal dynamics are sensitive to the seasonal and interannual morphological changes in the Qiantang Estuary. At smaller timescales (e.g., spring-neap cycle) the variation of SSC has significant influence on the tidal dynamics. This implies that river-tidal dynamic models for this estuary must include sediment dynamics and morphodynamics.

6. Conclusions

Based on long-term datasets of water levels at representative tidal gauging stations, river discharge and bathymetrical data in the estuary, the temporal-spatial variations and controls of the water levels were analyzed. The findings are summarized below.

Within a spring-neap tidal cycle, tidal amplification in the upper estuary correlates positively with the tidal range at the mouth, due to the high sediment concentration at the middle reach and the variation of water depth in the upper reach.

On the seasonal and interannual timescales, the direct influence of river discharge on the tidal dynamics in the estuary is insignificant and restricted to elevating the highwater level in the upper estuary. On the other hand, the variation of river discharge plays an important indirect role on the tidal dynamics by triggering active morphological evolutions.

At the upper estuary, the tidal range and the amplification factor during high flow season or years can be more than double of those during the low flow season or years. During the low flow periods, the bed is gradually recovered, and the tidal range and amplification decrease. The flood dominance increases and decreases in the high and low flow periods, respectively. In the lower estuary, the flood dominance increases continuously, due to the morphological response to the large-scale embankment project.

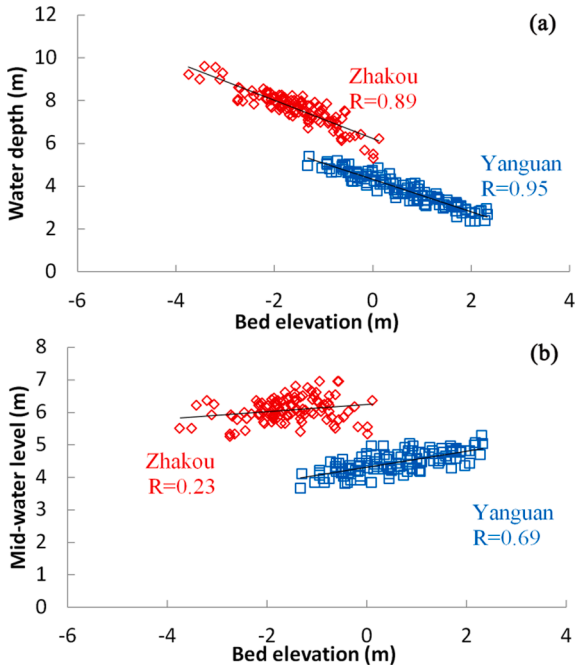

Fig. 15. Relationships between the cross-sectional water depths under the mid-water levels (a) and the monthly mid-water levels (b) at Zhakou and Yanguan and their bed elevations.

A conceptual model of river-tide-morphology interaction under natural conditions is proposed for estuaries with fast morphological evolutions.

Declaration of Competing Interest

The authors declare that they have no known competing financial interests or personal relationships that could have appeared to influence the work reported in this paper.

Acknowledgements:

This research was financed by the National Natural Science Foundation of China (No. 41676085; 42176170; 42076178), Major project of Zhejiang Provincial Natural Science Foundation (LZJWD22E090002), the Zhejiang Provincial Hydraulic Science and Technology Planning Project (No. RB2033), and the Dutch Royal Academy of Sciences via the project Coping with Deltas in Transition (No. PSA-SA-E-02) within the framework of Program Strategic Scientific Alliances between China and the Netherlands. We also wish to thank the two anonymous reviewers for their constructive comments which improved this work greatly.

References

Bolle, A., Bing Wang, Z., Amos, C., De Ronde, J., 2010. The influence of changes in tidal asymmetry on residual sediment transport in the Western Scheldt. Cont. Shelf Res. 30 (8), 871–882.

Burchard, H., Schuttelaars, H.M., 2012. Analysis of tidal straining as driver for estuarine circulation in well-mixed estuaries. J. Phys. Oceanogr. 42 (2), 261–271.

Cai, H., Savenije, H.H.G., Yang, Q., Ou, S., Lei, Y., 2012. Influence of river discharge and dredging on tidal wave propagation: Modaomen Estuary case. J. Hydraul. Eng. 138 (10), 885–896.

Cai, H., Savenije, H.H.G., Zuo, S., Jiang, C., Chua, V.P., 2015. A predictive model for salt intrusion in estuaries applied to the Yangtze estuary. J. Hydrol. 529, 1336–1349.

Cai, H., Savenije, H.H.G., Garel, E., Zhang, X., Guo, L., Zhang, M., Liu, F., Yang, Q., 2020. Seasonal behaviour of tidal damping and residual water level slope in the Yangtze River estuary: identifying the critical position and river discharge for maximum tidal damping. Hydrol. Earth Sys. Sci. 23 (6), 2779–2794.

Cao, Y.u., Zhang, W., Zhu, Y., Ji, X., Xu, Y., Wu, Y., Hoitink, A.J.F., 2020. Impact of trends in river discharge and ocean tides on water level dynamics in the Pearl River Delta. Coast. Eng. 157, 103634. https://doi.org/10.1016/j.coastaleng.2020.103634.

Chen, J., Liu, C., Zhang, C., Walker, H., 1990. Geomorphological development and sedimentation in Qiantang Estuary and Hangzhou Bay. J. Coastal Res. 6 (3), 559–572.
Chen, S., Han, Z., Hu, G., 2006. Impact of human activities on the river reach in the Qiantang Estuary (in Chinese with English abstract). J. Sediment. Res. 4, 61–67.
Choi, K., Kim, D., Jo, J., 2020. Morphodynamic evolution of the macrotidal Sittaung River estuary, Myanmar: Tidal versus seasonal controls. Mari. Geol. 430, 106367. https://doi.org/10.1016/j.margeo.2020.106367.
Cloern, J.E., 1987. Turbidity as a control on phytoplankton biomass and productivity in estuaries. Cont. Shelf Res. 7 (11-12), 1367–1381.
Cooper, J.A.G., 2002. The role of extreme floods in estuary-coastal behaviour: contrasts between river- and tide-dominated microtidal estuaries. Sed. Geol. 150 (1-2), 123–137.
Dai, Z.J., 2021. Changjiang riverine and estuarine hydro-morphodynamic processes: in the context of anthropocene era. Springer.
Dalrymple, R.W., Choi, K., 2007. Morphologic and facies trends through the fluvial-marine transition in tide-dominated depositional systems: a schematic framework for environmental and sequence-stratigraphic interpretation. Earth Sci. Rev. 81 (3-4), 135–174.
Dijkstra, Y.M., Schuttelaars, H.M., Schramkowski, G.P., Brouwer, R.L., 2019. Modeling the transition to high sediment concentrations as a response to channel deepening in the Ems River Estuary. J. Geophys Res. Oceans 124 (3), 1578–1594.
Dronkers, J., 1986. Tide-induced residual transport of fine sediment. Phys. Shall. Estua. Bay. 228–244.
Editorial Committee for Chinese Harbors and Embayment (ECCHE), 1992. Chinese harbors and embayment (Part V). China Ocean Press, Beijing (in Chinese).
Fan, D., Tu, J., Shang, S., Cai, G., 2014. Characteristics of tidal-bore deposits and facies associations in the Qiantang Estuary. China. Mar. Geol. 348, 1–14.
Fan, D., Wu, Y., Zhang, Y., Burr, G., Huo, M., Li, J., 2017. South flank of the Yangtze Delta: past, present, and future. Mar. Geol. 392, 78–93.
Friedrichs, C.T., Aubrey, D.G., 1988. Non-linear tidal distortion in shallow well-mixed estuaries: a synthesis. Estu. Coast. Shelf Sci. 27 (5), 521–545.
Friedrichs, C.T., Aubrey, D.G., 1994. Tidal propagation in strongly convergent channels. J. Geophys. Res. 99 (C2), 3321. https://doi.org/10.1029/93JC03219.
Friedrichs, C., Madsen, O., 1992. Nonlinear diffusion of the tidal signal in frictionally dominated embayments. J. Geophys. Res. 97 (N3C4), 5637–5650.
Gao, S., Wang, Y., 2008. Material fluxes from the Changjiang River and their implications on the adjoining continental shelf ecosystem. Cont. Shelf Res. 28, 1490–1500.
Godin, G., 1991. Frictional effects in river tides. In: Parker, B.B. (Ed.), Progress in Tidal Hydrodynamics. John Wiley, New York, pp. 379–402.
Guo, L., van der Wegen, M., Jay, D.A., Matte, P., Wang, Z.B., Roelvink, D., He, Q., 2015. River-tide dynamics: Exploration of nonstationary and nonlinear tidal behavior in the Yangtze River estuary. J. Geophys. Res. Oceans 120 (5), 3499–3521.
Guo, L., Wang, Z.B., Townend, I., He, Q., 2019. Quantification of tidal asymmetry and its nonstationary variations. J. Geophys. Res. Oceans 124 (1), 773–787.
Han, Z., Cao, Y., You, A., 2009. Verification of fluvio-morphology for macro-tide estuary with tidal bore (in Chinese with English abstract). Hydro-Sci. Eng. 4, 83–90.
Han, Z., Dai, Z., Li, G., 2003. Regulation and Exploitation of Qiantang Estuary (in Chinese). China Water Power Press, Beijing.
Hoitink, A.J.F., Jay, D.A., 2016. Tidal river dynamics: Implications for deltas. Rev. Geophys. 54 (1), 240–272.
Hoitink, A.J.F., Wang, Z.B., Vermeulen, B., Huismans, Y., Kästner, K., 2017. Tidal controls on river delta morphology. Nature Geosci. 10 (9), 637–645.
Hu, P., Han, J.J., Li, W., Sun, Z.L., He, Z.G., 2018. Numerical investigation of a sandbar formation and evolution in a tide-dominated estuary using a hydro-sediment-morphodynamic model. Coast. Eng. J. 60 (4), 466–483.
Huang, J.B., Xie, D.F., 2020. Detecting the river-sea influenced boundary changes in a macro-tidal estuary based on morphodynamic modeling. J. Coast. Res. 104, 804–812.
Jalón-Rojas, I., Sottolichio, A., Hanquiez, V., Fort, A., Schmidt, S., 2018. To what extent multidecadal changes in morphology and fluvial discharge impact tide in a convergent (turbid) tidal river. J. Geophys. Res. Oceans 123 (5), 3241–3258.
Jay, D.A., 1991. Green's law revisited: Tidal long-wave propagation in channels with strong topography. J. Geophys. Res. 96 (C11), 20585. https://doi.org/10.1029/91JC01633.
Jay, D.A., Leffler, K., Degens, S., 2011. Long-term evolution of Columbia River tides. J. Water. Port Coast. Ocean Eng. 137 (4), 182–191.
Kukulka, T., Jay, D.A., 2003a. Impacts of Columbia River discharge on salmonid habitat: 1. A nonstationary fluvial tide model. J. Geophys. Res. 108 (C9), 3293.
Kukulka, T., Jay, D.A., 2003b. Impacts of Columbia River discharge on salmonid habitat: 2. Changes in shallow-water habitat. J. Geophys. Res. 108 (C9), 3294.
Li, L.i., He, Z., Xia, Y., Dou, X., 2018. Dynamics of sediment transport and stratification in Changjiang River Estuary. China. Estu. Coast. Shelf Sci. 213, 1–17.
Lin, C.-M., Zhuo, H.-C., Gao, S., 2005. Sedimentary facies and evolution in the Qiantang River incised valley, eastern China. Mar. Geol. 219 (4), 235–259.
Lin, S., Xu, Y.P., Tian, Y., Lou, Z.H., 2012. Spatial and temporal analysis of drought in Qiantang River basin based on Z index and SPI (in Chinese with English abstract). J. Hydroelec. Eng. 31 (2), 20–26.
Luan, H.L., Ding, P.X., Wang, Z.B., Ge, J.Z., Yang, S.L., 2016. Decadal morphological evolution of the Yangtze Estuary in response to river input changes and estuarine engineering projects. Geomorphology 265, 12–23.
Matte, P., Secretan, Y., Morin, J., 2014. Temporal and spatial variability of tidal-fluvial dynamics in the St. Lawrence fluvial estuary: an application of nonstationary tidal harmonic analysis. J. Geophys. Res. Oceans 119 (9), 5724–5744.
Munk, W.H., Cartwright, D.E., 1966. Tidal spectroscopy and predication. Philos. Trans. R. Soc. Lond. Ser. A. 259, 533–581.
Pan, C.-H., Lin, B.-Y., Mao, X.-Z., 2007. Case Study: Numerical Modeling of the Tidal Bore on the Qiantang River, China. J. Hydrau. Eng. 133 (2), 130–138.
Pan, C., Zheng, J., Chen, G., He, C., Tang, Z., 2019. Spatial and temporal variations of tide characteristics in Hangzhou Bay and cause analysis (in Chinese with English Abstract). Ocean Eng. 37 (3), 1–11.
Pan, C., Huang, W., 2010. Numerical modeling of suspended sediment transport in Qiantang River: An estuary affected by tidal bore. J. Coast. Res. 26, 1123–1132.
Sassi, M.G., Hoitink, A.J.F., 2013. River flow controls on tides and tide-mean water level profiles in a tidal freshwater river. J. Geophys. Res. Oceans 118 (9), 4139–4151.
Savenije, H.H.G., 2012. Salinity and tides in alluvial estuaries, completely revised 2nd edition, http://www.salinityandtides.com.
Shaw, J.B., Mohrig, D., 2014. The importance of erosion in distributary channel network growth, Wax Lake Delta, Louisiana, USA. Geology 42 (1), 31–34.
Shimozono, T., Tajima, Y., Akamatsu, S., Matsuba, Y., Kawasaki, A., 2019. Large-scale channel migration in the Sittang River Estuary. Sci. Rep. 9, 9862.
Smith, T.R., 1974. A derivation of the hydraulic geometry of steady-state channels from conservation principles and sediment transport laws. J. Geol. 82 (1), 98–104.
Song, D., Wang, X.H., Zhu, X., Bao, X., 2013. Modeling studies of the far-field effects of tidal flat reclamation on tidal dynamics in the East China Seas. Estuar. Coast. Shelf Sci. 133, 147–160.
Syvitski, J.P.M., Kettner, A.J., Overeem, I., Hutton, E.W.H., Hannon, M.T., Brakenridge, G.R., Day, J., Vörösmarty, C., Saito, Y., Giosan, L., Nicholls, R.J., 2009. Sinking deltas due to human activities. Nat. Geosci. 2 (10), 681–686.
Talke, S.A., Jay, D.A., 2020. Changing tides: The role of natural and anthropogenic factors. Ann. Rev. Mar. Sci. 12 (1), 121–151.
Talke, S.A., de Swart, H.E., de Jonge, V.N., 2009. An idealized model and systematic process study of oxygen depletion in highly turbid estuaries. Estu. Coast. 32 (4), 602–620.
Tian, Y.e., Xu, Y.-P., Booij, M.J., Lin, S., Zhang, Q., Lou, Z., 2012. Detection of trends in precipitation extremes in Zhejiang, east China. Theor. Appl. Climatol. 107 (1-2), 201–210.
Toublanc, F., Brenon, I., Coulombier, T., Le Moine, O., 2015. Fortnightly tidal asymmetry inversions and perspectives on sediment dynamics in a macrotidal estuary (Charente, France). Cont. Shelf Res. 94, 42–54.
Tu, J., Fan, D., 2017. Flow and turbulence structure in a hypertidal estuary with the world's biggest tidal bore. J. Geophys. Res. Oceans 122 (4), 3417–3433.
Uncles, R.J., Joint, I., Stephens, J.A., 1998. Transport and retention of suspended particulate matter and bacteria in the Humber-Ouse Estuary, United Kingdom, and their relationship to hypoxia and anoxia. Estuaries 21 (4), 597. https://doi.org/10.2307/1353298.
van der Wal, D., Pye, K., Neal, A., 2002. Long-term morphological change in the Ribble estuary, Northwest England. Mar. Geol. 189 (3-4), 249–266.
van Maren, D.S., Winterwerp, J.C., Vroom, J., 2015. Fine sediment transport into the hyper-turbid lower Ems River: The role of channel deepening and sediment-induced drag reduction. Ocean Dyn. 65 (4), 589–605.
Wang, Z.B., Jeuken, M.C.J.L., Gerritsen, H., de Vriend, H.J., Kornman, B.A., 2002. Morphology and asymmetry of the vertical tide in the Westerschelde estuary. Cont. Shelf Res. 22 (17), 2599–2609.
Wang, Z.B., Vandenbruwaene, W., Taal, M., Winterwerp, H., 2019. Amplification and deformation of tidal wave in the Upper Scheldt Estuary. Ocean Dyn. 69 (7), 829–839.
Wang, Z.B., Winterwerp, J.C., He, Q., 2014. Interaction between suspended sediment and tidal amplification in the Guadalquivir Estuary. Ocean Dyn. 64 (10), 1487–1498.
Winterwerp, J.C., Wang, Z.B., van Braeckel, A., van Holland, G., Kösters, F., 2013. Man-induced regime shifts in small estuaries-II: a comparison of rivers. Ocean Dyn. 63 (11-12), 1293–1306.
Winterwerp, J.C., Wang, Z.B., 2013. Man-induced regime shifts in small estuaries-I: Theory. Ocean Dyn. 63 (11-12), 1279–1292.
Xia, F., Liu, X., Xu, J., Xu, L., Shi., Z., 2016. Precipitation change between 1960 and 2006 in the Qiantang River basin, Ease China. Climat. Res. 67, 257–-269.
Xie, D., Gao, S., Wang, Z.B., Pan, C., Wu, X., Wang, Q., 2017a. Morphodynamic modeling of a large inside sandbar and its dextral morphology in a convergent estuary: Qiantang Estuary. China. J. Geophys. Res. Earth Surf. 122 (8), 1553–1572.
Xie, D., Pan, C., Wu, X., Gao, S., Wang, Z.B., 2017b. Local human activities overwhelm decreased sediment supply from the Changjiang River: Continued rapid accumulation in the Hangzhou Bay-Qiantang Estuary system. Mar. Geol. 392, 66–77.
Xie, D., Pan, C., Gao, S., Wang, Z.B., 2018. Morphodynamics of the Qiantang Estuary, China: Controls of river flood events and tidal bores. Mar. Geol. 406, 27–33.
Xie, D., Huang, J., Bo, J., Li, R., Tang, Z., Lu, H., 2020. A preliminary study on seasonal variations of sediment concentrations in the inner Qiantang Estuary. IOP Conf. Ser.: Earth Environ. Sci. 569 (1), 012079. https://doi.org/10.1088/1755-1315/569/1/012079.
Xie, D., Wang, Z.B., Van der Wegen, M., Huang, J., 2021. Morphodynamic modeling the impact of large-scale embankment on the large bar in a convergent estuary. Mar. Geol. 442, 106638. https://doi.org/10.1016/j.margeo.2021.106638.
Yu, Q., Wang, Y., Gao, S., Flemming, B., 2012. Modeling the formation of a sand bar within a large funnel-shaped, tide-dominated estuary: Qiantangjiang Estuary. China. Mar. Geol. 299-302, 63–76.
Zeng, J., Chen, G., Pan, C., Zhang, Z., 2017. Effect of dike adjustment on the tidal bore in the Qiantang Estuary. China. J. Hydrodyn. 27 (3), 452–459.
Zeng, J., Sun, Z.L., Pan, C.H., Chen, G., 2010. Long-periodic feature of runoff and its effect o riverbed in Qiantang estuary (in Chinese with English abstract). J. Zhejiang Uni. (Eng. Sci.) 44 (8), 1584–1588.
Zhang, M., Townend, I., Zhou, Y., Cai, H., 2016. Seasonal variation of river and tide energy in the Yangtze estuary. China. Earth Surf. Proc. Land. 41 (1), 98–116.

Zhang, W., Cao, Y.u., Zhu, Y., Zheng, J., Ji, X., Xu, Y., Wu, Y., Hoitink, A.J.F., 2018. Unravelling the causes of tidal asymmetry in deltas. J. Hydrol. 564, 588–604.
Zhang, W., Ruan, X., Zheng, J., Zhu, Y., Wu, H., 2010. Long-term change in tidal dynamics and its cause in the Pearl River Delta. China. Geomorphology 120 (3-4), 209–223.
Zhang, X., Dalrymple, R.W., Yang, S.-Y., Lin, C.-M., Wang, P., 2015b. Provenance of Holocene sediments in the outer part of the paleo-Qiantang River estuary. China. Mar. Geol. 366, 1–15.
Zhou, Z., Coco, G., Townend, I., Gong, Z., Wang, Z., Zhang, C., 2018. On the stability relationships between tidal asymmetry and morphologies of tidal basins and estuaries. Earth Surf. Process. Land. 43 (9), 1943–1959.